Applied Energy 254 (2019) 113666

Contents lists available at ScienceDirect

Applied Energy

journal homepage: www.elsevier.com/locate/apenergy

Accounting for subsurface uncertainty in enhanced geothermal systems to make more robust techno-economic decisions

Ahinoam Pollack*, Tapan Mukerji

Stanford University, 367 Panama St, Stanford, CA 94305, USA

HIGHLIGHTS

- Analysis of the influence of subsurface uncertainty on Enhanced Geothermal Systems.
- Two workflow for optimizing Enhanced Geothermal Systems were tested.
- Optimization using a single earth model leads to overly optimistic predictions.
- Optimization using an ensemble of earth models shows realistic uncertainty ranges.
- More robust engineering decisions are validated using multiple earth models.

ARTICLE INFO

Keywords:
Enhanced geothermal system
Sensitivity analysis
Hydraulic fracturing
Uncertainty quantification

ABSTRACT

It has been estimated that Enhanced Geothermal Systems could supply 100 GWe (10%) of total electric capacity in the U.S. An Enhanced Geothermal System (EGS) is created by stimulating an impermeable hot rock, injecting cold water into the hot reservoir, and extracting the heated water to generate electricity. EGS projects are still not commercially feasible, however, due to many challenges, including subsurface uncertainty. There are many uncertain structural and geological features when creating an EGS. With uncertain reservoir properties, it is difficult to optimize decisions that will greatly improve EGS profitability. Currently, a common method of optimizing an EGS is choosing the most representative subsurface reservoir model and optimizing the engineering parameters for this single reservoir model, or Single-Model Optimization (SM-Opt). Due to availability of larger computational power, another feasible option is accounting for subsurface uncertainty by optimizing an EGS given an ensemble of reservoir models, or Multiple Model Optimization (MM-Opt). This option is less common in practice within the geothermal industry since it lags in harnessing computational power. This study compares these two methods for optimizing eight common EGS engineering decisions, including well configuration and fracture spacing. The decisions were optimized to maximize the Net Present Value (NPV) of an EGS. We have found that using SM-Opt, the optimal engineering decisions led to an EGS with a NPV estimate of $32.7 million. This contrasts with the MM-Opt results where the optimal engineering decisions led to a median NPV value of $11 million and a standard deviation of $15 million. This comparison illustrates how ignoring subsurface uncertainty and heterogeneity leads to over-optimistic NPV forecasts. For this study, the SM-Opt optimum decisions were similar to the robust decisions identified using MM-Opt. Yet, in contrast to SM-Opt, the MM-Opt workflow provided an analysis of the influential engineering parameters and a NPV uncertainty range, which was used to ensure decision robustness.

1. Introduction – enhanced geothermal systems (EGS)

Sixty-five percent of greenhouse gas emissions result from fossil fuel combustion and industrial processes [1]. To mitigate global warming, we must reduce the use of fossil fuels and transition into low carbon renewable energy sources. Solar and wind energy facilities are rapidly expanding but are insufficient as sole energy sources due to their intermittency and dependence on weather conditions. Geothermal energy is a clean (almost zero carbon emissions) renewable energy that can complement fluctuating renewable sources by operating flexibly and providing energy at times when there is insufficient contribution from solar and wind energy.

Currently, geothermal energy provides only 0.2% of the total U.S. energy consumption [2]. The expansion capability of geothermal

* Corresponding author.
E-mail address: ahinoamp@stanford.edu (A. Pollack).

https://doi.org/10.1016/j.apenergy.2019.113666
Received 23 January 2019; Received in revised form 24 July 2019; Accepted 1 August 2019
Available online 21 August 2019

energy is limited in both size and geography to areas with certain characteristics. Conventional geothermal systems (hydrothermal systems) require three criteria: a source of high temperature, in-situ water, and a permeable reservoir. In hydrothermal systems, sources of high temperature, such as magmatic bodies or hot deep basement rocks, heat up in-situ water inside naturally fractured or porous water reservoirs. Geothermal power plants extract the heated water to generate electricity. Natural hydrothermal systems with all three characteristics, however, are rare. There are few tectonically and volcanically active locations on earth with a heat source sufficiently close to a permeable water aquifer.

EGS projects offer the opportunity to engineer geothermal systems in locations without a natural geothermal system. There are many subsurface locations on earth that have a sufficiently high temperature, but lack in-situ water and permeability to become a geothermal resource. Usually, from 3 to 6 km beneath the earth's surface, there are rock formations hot enough (150–250 °C) to be a thermal resource for geothermal energy. The thermal energy of such rocks can be harvested in an EGS. First tested in Los Alamos National Laboratory in 1972, an EGS is an artificial geothermal system, similar to a heat exchange circuit.

Typically, an initial exploration well already exists on a prospective EGS site and this well provides data about the temperature, faulting and lithology in the subsurface in the vicinity of the well (Fig. 1(a)). Following data analysis, an injection well is drilled into hot rocks (Fig. 1(b)). Pressurized fluid is injected through the injection well to induce shear slip and open pre-existing fractures or create tensile fractures. The fracture networks form a permeable reservoir. Next, production wells are drilled to intersect the stimulated zone around the injection well (Fig. 1(c)). Cold fluid is then injected into the subsurface via the injection wells and heats up as it circulates though hot rocks in the fractured reservoir. The fluid is then pumped out of production wells and powers turbines to generate electricity. The cooled fluid is then reinjected into the subsurface.

An EGS creates the necessary permeability needed for a geothermal reservoir and supplies the necessary circulating water from outside the reservoir (perhaps a nearby saline aquifer). Thus, an EGS can be constructed anywhere with hot rocks at depth, which opens almost any area on earth for possible EGS development. Recent research has argued that EGS could supply 100 GWe (10%) of total electric capacity in the U.S. [3].

1.1. Challenge: subsurface uncertainty

EGS is still not commercially feasible due to many challenges. This paper will focus on the subsurface related challenges, specifically the issue of optimizing the design of an EGS given subsurface uncertainty, which is a major challenge in the geothermal industry. There are many uncertain subsurface parameters when creating an EGS. Uncertain geological and structural parameters include the stress field, location and orientation of natural fractures and faults, and temperature and pressure distribution. Therefore, the reservoir's response to engineering decisions cannot be predicted with certainty using numerical simulators since the subsurface properties necessary as input to run the simulators are uncertain. In addition, the physical mechanisms governing fracture creation are still being researched. With an uncertain reservoir response, it is challenging to make engineering optimization decisions that would greatly improve the profitability of an EGS.

This uncertainty regarding the operating setting is unique to subsurface environments compared to other renewable projects. For example, when designing a solar panel, the environmental criteria, such as solar radiation and cloud cover at a particular site, can be measured at relatively low cost. In geothermal systems, measuring the temperature and relevant rock properties in the subsurface in a single location requires drilling a multimillion dollar well. Furthermore, a single drilled well is still insufficient for fully characterizing the properties of the reservoir at a distance from the wellbore. Without full knowledge of subsurface properties, it is difficult to optimize engineering decisions.

1.2. Decision making given subsurface uncertainty

The process of creating an EGS involves a series of decisions based

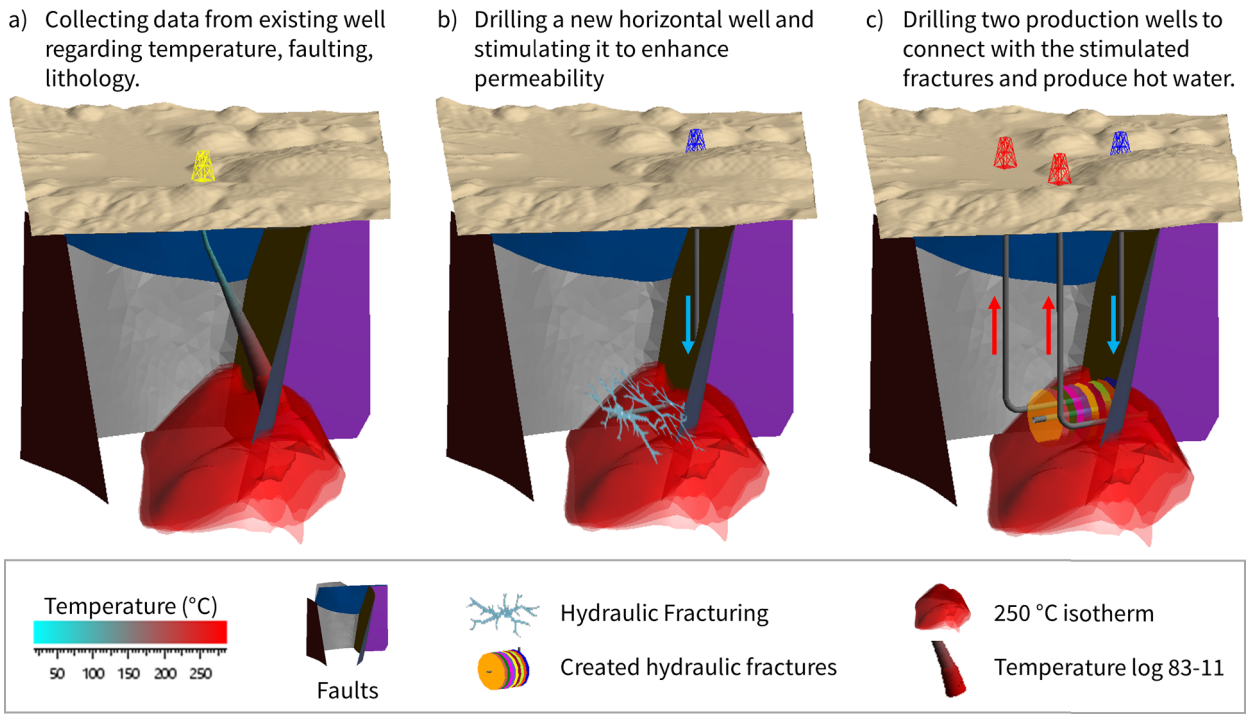

Fig. 1. Schematic of the process of creating an EGS site. (a) An initial exploration well provides data about the subsurface. (b) An injection well is drilled into a hot area of the subsurface (near the 250 °C isotherm). The injection well is hydraulically fractured to increase permeability and create a fractured reservoir. (c) Cold water injected via an injector well (blue arrow) heats up as it travels through stimulated hydraulic fractures (colored circles) from the injector to the two producers (red arrows). The hot fluid is used to generate electricity. Faulting and well data based on Coso site data [21].

on limited data. In this section, we review some of the different decisions that need to be made in the process of creating an EGS, the data that is necessary to make those decisions, and the data that is available to make those decisions.

Initially, an exploration-well provides data regarding temperature, faulting and lithology near the wellbore. After reviewing the exploration-well data, the developer needs to decide where to drill the main injection well. To make such a decision, the developer would ideally know the distribution of temperature throughout the subsurface. This temperature distribution, however, cannot be measured. Only the temperature at the exploration wellbore is known, but not the spatial extension of the temperature away from the wellbore. In addition, the developer needs to decide whether to place the wellbore near or away from an existing fault. However, this depends on the fault properties and geometry, which are mostly unknown. The developer also needs to decide the extent of the horizontal section of the wellbore and the wellbore diameter, but needs to know how much additional profit would be generated from having a longer or a wider wellbore to make such a decision. The profitability of the system, though, depends on the success of the stimulation, which is extremely difficult to predict, since the subsurface rock properties and pre-existing fractures are unknown.

After drilling an injection well, the developer needs to decide how to perform the hydraulic fracturing. Specifically, what should be the spacing between every fracture cluster. To make such a decision, the developer would need to perform a cost-benefit analysis since increasing the cluster density would cost more money. Estimates of the financial benefit of increasing the cluster density can come either from similar sites that performed hydraulic fracturing or from numerical modeling, which depend highly on unknown rock properties and distribution of pre-existing faults.

After stimulation, the developer needs to decide where to place the production wells such that they will intersect the zone of stimulated rock created during the hydraulic fracturing process. Microearthquake monitoring can give a general idea regarding the zone of stimulation, but recent research has found that the microseismicity cloud can be substantially larger than the associated stimulated fracture volume [4]. The developer can only know the approximate extension of the stimulated fracture volume.

Once the production wells are in place, the developer needs to choose operating pressures for the wellbores in such a way as to avoid thermal breakthrough. Information about future thermal breakthrough can possibly be gained by tracer testing after the system is running. The correlation between tracer returns and thermal breakthrough time is an active research topic and can only provide a range of possible future thermal breakthrough times.

The engineering decisions necessary within an EGS project are summarized in Table 1. They highlight a challenging problem of creating a subsurface system with incomplete information about the properties and structure of the subsurface. In industry, geoscientists commonly tackle this problem by using all the available data to make a single interpretation, or single model, of the subsurface that provides a single estimate of the unknown earth properties in the subsurface. That subsurface model is then used to make predictions and decide on the optimal engineering decisions.

Historically, the tactic of creating a single interpretation of the subsurface has led to decisions that are not robust to uncertain earth properties. For example, at the initial Fenton Hill site, geoscientists assumed the hydraulic fractures were going to propagate in a certain direction for a predetermined distance based on a stress measurement at a single location. Therefore, they drilled both the injection and production wells at the same time, assuming the future hydraulic fractures would connect the two wells. The hydraulic fractures did not propagate in the anticipated direction, and there was no flow connection established between the injection and production wells. It was determined that there was an unanticipated shift in the stress field [3]. The decision to drill two wells based on a single interpretation of a homogenous stress field led to decisions that were not robust in the face of uncertainty. A similar scenario to that described above occurred in an EGS site in Rosemanowes. Two wells were drilled based on a single interpretation of the subsurface properties and the wells did not connect due to unexpected previously existing fractures [3].

Both of the above examples show that the current strategy of relying on a single interpretation of the available data does not create EGS projects that are robust in the face of unexpected subsurface properties. In the past, it was probably computationally unfeasible to consider many different models of the subsurface and find engineering decisions that are robust to multiple different earth scenarios. Now, with the recent advent of high performance computing, such methodology is possible. In this paper, we examine the advantages of optimizing EGS projects given multiple earth models.

1.3. Different methods to optimize an EGS

There are two common methods for optimizing the engineering decisions described in the previous section:

- **Single Model Optimization (SM-Opt):** Performing deterministic interpretations and modeling (ignoring ranges of uncertainty) to arrive at the most representative earth model with the most likely values of subsurface properties. Then, using this reservoir model to find the engineering decisions that maximize Net Present Value (NPV).
- **Multiple Model Optimization (MM-Opt):** Assessing the ranges of uncertainty of the subsurface properties and creating an ensemble of reservoir models that are possible given the subsurface uncertainty. Performing an optimization on this ensemble of reservoir models.

MM-Opt requires a much larger number of simulations as compared to SM-Opt. By simulating the EGS performance given the varying subsurface parameters, MM-Opt methods can quantify the uncertainty of EGS performance. It is not clear, however, whether MM-Opt can actually lead to more robust reservoir engineering decisions. This paper will use both MM-Opt and SM-Opt to optimize the NPV of a hypothetical EGS in California to determine the differences in the results of the optimization workflow.

1.4. Previous research on optimizing an EGS given subsurface uncertainty

Previous literature on this topic has mostly been divided into two groups: one group focusing on optimizing engineering decisions in an EGS given a single reservoir model, and another group focusing on quantifying and reducing the uncertainty of subsurface parameters given data.

Li et al. [5] performed an optimization and sensitivity analysis of an EGS design with a single horizontal well injector and a single horizontal well producer. Li found that increasing the number of fractures increases the possible flow rate through the system, since the effective permeability in the system increases linearly with the number of fractures. Asai et al. [6] studied the dominant factors affecting the performance of an EGS, finding that a large distance between the production and injection well is the most important variable. A low injection temperature and a high total flow rate were also found to be impactful. Song et al. [7] tested a set of varying configurations of multi-lateral wells given a constant reservoir model, showing that different well configurations can lead to different energy outputs. All the above studies, however, assumed a model where all the stimulated fractures have a constant fracture aperture and length.

Doe et al. [8], on the other hand, discussed more realistic scenarios where the stimulated fractures have variable fracture apertures and how that variability affects EGS performance. Doe et al. show that variability in fracture apertures leads to preferential flow paths, where the flow concentrates in fractures with anomalously high apertures, which causes early thermal breakthrough. Similarly, Guo et al. [9] show that even inside every single fracture there is aperture variability that leads to preferential pathways and thermal short circuiting.

EGS optimization work by both Hu et al. [10] and Hofmann et al. [11] focused more on optimizing the stimulation of the hydraulic fractures. Hofmann et al. showed the importance of mechanical rock

Table 1
Table of decisions made in the process of creating an EGS, the information needed to make those decisions, and the actual information available.

Decision	Information needed	Information available
Where to drill the injection well? Should one drill the well near an existing fault?	The distribution of temperature, stress, pressure, lithology, in the subsurface. The effect of the natural fault on production.	Temperature, pressure, stress and lithology data along a wellbore, with little information regarding the surrounding rock.
How long to make the horizontal length of the well?	The extra revenue that will be generated from each additional length of wellbore. This is dependent on the success of fracturing.	Information about the future success of hydraulic fracturing can come from either similar sites that performed hydraulic fracturing or from numerical modeling, which necessitates input of unknown rock properties and distribution of pre-existing faults.
How to hydraulically fracture the well? What should be the fracture spacing?	The extra revenue that will be generated from each fracture cluster.	Same as above.
Where to place the production wells? How far away from the injection well?	To decide how far to place the production wells, one needs to know how far the hydraulic fractures extended.	Microearthquake monitoring can give a general idea regarding the zone of stimulation, but recent research has found that the Microseismicity cloud can be substantially larger than the associated stimulated fracture volume [4].
What diameters should the injection and production wells be?	The amount of fluid that will be produced from the system, which depends on the in-situ condition and the stimulation results.	Information about future production flow rates can perhaps come from flow/injection tests of the injection well after stimulation. Though this would not be very informative since the important parameter is the flow connectivity achieved between the wells, which is unknown until after the two production wells are drilled.
At what pressures to operate the production and injection wells?	The likelihood of causing thermal breakthrough, which depends on the flow network.	Information about future thermal breakthrough can possibly be gained by tracer testing after the system is running. The correlation between tracer testing and thermal breakthrough time is an active research topic.

properties, stress confinement, and pre-existing natural fractures for creating large fracture network areas. An important insight from Hu's work is the hydraulic fractures' sensitivity to stress anisotropy, natural fracture distribution, and stress shadowing effects. The fractures in Hu's simulations have variable lengths, heights, apertures, and directions. The above optimization studies highlight the sensitivity of hydraulic fractures' geometries and properties to the relatively unknown and possibly heterogeneous subsurface stress state.

The afore cited research focused on EGS optimization. There is also a large amount of literature on the uncertainty of reservoir properties in an EGS and methods to reduce the uncertainty using stochastic inversion of acquired data. Vogt et al. [12] uses Monte Carlo methods together with Sequential Gaussian Simulation and observed borehole data to estimate the thermal conductivity field at a potential geothermal site in the Hague, Netherlands. In addition, Vogt uses Sequential Gaussian Simulation to simulate the permeability field of faults at the Soultz site, then simulates the flow field, and uses rejection sampling to find earth models that match the observed tracer returns [13]. Tompson et al. [14] and Melleros et al. [15] perform a joint sequential inversion of resistivity data and temperature borehole data using MCMC methods to attain plausible realizations of the temperature, pressure and resistivity fields at Superstition Mountain, California. Cui et al. [16] use an adaptive delayed acceptance Metropolis Hastings algorithm to calibrate a geothermal reservoir model given temperature borehole data. Several papers have been written on the use of an Ensemble Kalman Filter to integrate observed and prior model data to update the range of uncertainty of reservoir properties in geothermal systems [17–19].

There has been significant work done on optimizing EGS engineering parameters given a constant reservoir model and quantifying the uncertainty of reservoir models. Yet, there has been little work that combines both of these aspects and researches the optimization of EGS engineering parameters given the uncertain subsurface parameters. There is little discussion on making decisions in EGS projects that are robust in the face of uncertain reservoir properties.

2. Methodology

To determine the impact of using SM-Opt versus MM-Opt, we performed two separate workflows: Particle Swarm Optimization (PSO) [20] on a single reservoir model (SM-Opt), and Monte Carlo Optimization (exhaustive brute force sampling) given varying earth parameters (MM-Opt). These two workflows are described below and summarized visually in Fig. 2.

The SM-Opt workflow is as follows:

I. Choose the mean values of each of the uncertain earth parameters given in Table 2 and Table 3. These mean values are used to create a single supposedly most representative reservoir model.
II. Use any appropriate optimization algorithm to converge on the optimal engineering parameters that maximize the NPV of the EGS given the constant earth model.
   - Build a flow simulation model based on the constant reservoir model.
   - For each simulation, use the engineering parameters determined by the optimization algorithm. For this study, we used a PSO algorithm for the optimization process, with a population size of ten, a cognition component and social component of 1.5, and an inertia weight of 0.72.
   - Simulate the hydro-thermal flow and energy production for twenty years.
   - Calculate the NPV based on the energy production and associated costs.

The MM-Opt workflow is as follows:

I. Sample values from the distributions of uncertain earth parameters and engineering decisions, given in Tables 2–4. Build a flow simulation model based on each of the sampled earth parameters and engineering decisions. Simulate the hydro-thermal flow and energy production for twenty years. Calculate the NPV for each EGS simulation based on the simulated energy generation and financial model.
II. Examine the conditional probability distribution functions of NPV values given the different engineering decisions to determine optimal engineering parameter ranges.

For the hydro-thermal simulation, we used the commercial simulator CMG STARS [30]. We represented the hydraulic fractures as thin layers of porous media. Future work will explore the use of discrete fracture network representation and use of simulators that do not assume local thermal equilibrium [31,32].

2.1. The varying subsurface and engineering parameters

The numerical model for this sensitivity analysis was based on the West Flank of the Coso Geothermal Field in California. The West Flank

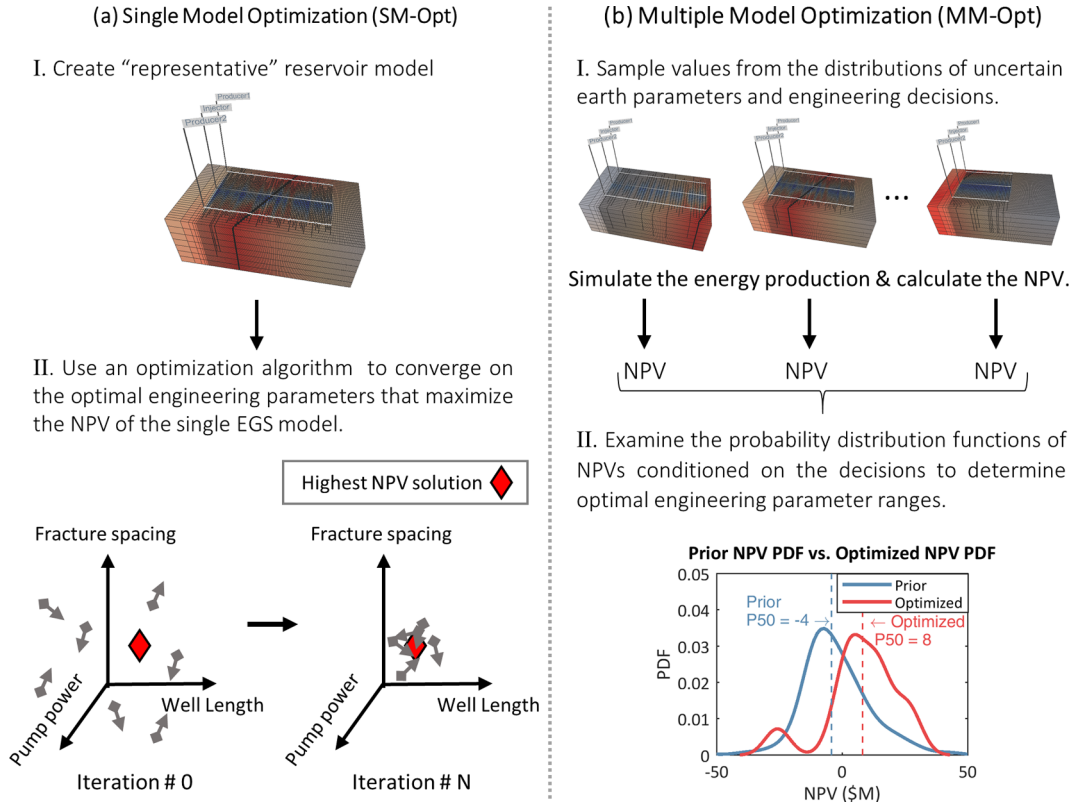

Fig. 2. Comparison of the two workflows used in this paper: (a) Single Model Optimization (SM-Opt) using PSO, and (b) Multiple Model Optimization (MM-Opt) using Monte Carlo optimization (exhaustive brute force sampling) and varying earth parameters.

has rock temperatures reaching 270 °C, but the formation is impermeable. In this study, we investigate a theoretical EGS built at this site. An example of a numerical representation of the EGS is shown in Fig. 4(a). The numerical model includes an injector flanked by two producers on either side. Hydraulic fractures of varying lengths, heights, and apertures connect the injector and the producers, as shown by the thin black lines in Fig. 4(a) and the square elements in Fig. 4(b). The hydraulic fractures in real field cases would be identified via microseismic monitoring. A natural fault present at Coso is included in the model.

The value ranges of the uncertain earth parameters for this study are based on the current uncertainty of those values after initial exploration at the Coso site, which is described in detail by Blankenship et al. [21]. Table 2 shows the ranges of uncertainty for the matrix parameters used in the numerical model.

The width of the hot zone around the fault is one of the important uncertain parameters. The temperature log for the site indicates an intersection with a natural fault, at which point the temperature rapidly increases. However, the distance at which the temperature falls off away from the fault is unknown and will affect the field's production. This temperature can be estimated by the following analytic equation, detailing the temperature falloff from a linear constant temperature boundary due to thermal diffusion [33]:

$$T^m(y, t) = T_0^m + (T_0^f - T_0^m)\,erfc\left(\frac{|y|}{2\sqrt{D_T t}}\right) \quad (1)$$

where T^m is the temperature of the matrix, T_0^m is the initial reservoir temperature, T_0^f is the temperature of the fault surface, D_T is the rock thermal diffusivity, y is the distance away from the fault along the fault normal, and t is the time during which there was convective flow throughout the fracture causing the thermal anomaly. In this study, the temperature falloff at a distance from the fault was modeled via the error function and a falloff distance, or "width of the hot zone around the fault." This distance is a function of the unknown length of time for which there was convective flow up the fault and the geological history of the area. Numerical studies have shown this this falloff distance away from the fault is variable [34]. An illustration of the parameterization of the width of the hot zone around the fault is shown in Fig. 3.

In the reservoir models, the hydraulic fractures were defined by an aspect ratio, half-length, and aperture. In reality, these hydraulic fracture properties are controlled by both the hydraulic fracturing process and the natural properties of the formation being fractured, including the stress state, fracture toughness, stress layering, and most importantly, the presence of natural fractures and faults in the formation. In this study, the hydraulic fractures were modeled as having properties that are a result of a random process. It is assumed that the properties of

Table 2
Uncertain matrix parameters.

Matrix Parameters	Distribution	Source of information
Matrix permeability (md)	log10(perm) → $U[-2,-5]$	Analysis in [21]
Rock heat capacity (kJ/(kg·K))	μ → U[0.8, 1.3]	The rock types are primarily rhyolite, diorite and granite. The typical heat capacity ranges for these rocks are from [22,23]
Rock thermal conductivity (W/(m·k))	μ → U[2,4]U	Typical thermal conductivity ranges for these rocks from [22,23]
Width of Hot Zone Around Fault (m)	U[200,1000]	Temperature logs; assumes heat source is hot water flow up fault
Matrix Porosity (unitless)	U[0.3, 1.6]	Typical fractured igneous rock porosity range based on [22]

Table 3
Uncertain fracture parameters.

Fracture Parameters	Distribution	Source of information
Hydraulic fracture half length (m)	$\mu \rightarrow U[100,300]$ $\sigma \rightarrow 0.2*\mu$	Ideally, this value would be taken from experiments at similar sites or rigorous simulations based on the measurements of the stress state. For now, values are guided by literature review and simulations done by [11] and [24]. Hydraulic fracturing with proppant at Groß Schönebeck in Germany initiated fractures with calculated half-length of 90 and 190 m [25]
Fracture aperture (m)	$\mu \rightarrow U[0.0005, 0.0018]$, $\sigma \rightarrow 0.2 * \mu$	Ranges are guided by [11] and [24]
Aspect ratio (mean fracture height/mean fracture length)	$\mu \rightarrow U[0.7, 1]$	Ranges are guided by [11] and [24]. Assumes an isotropic stress and fracture toughness field with little layering in the crystalline rock
Ratio of fracture vertical extent downward relative to upwards.	$\mu \rightarrow U[0.7, 0.95]$	Ranges are guided by [11] and [24]. Assumes possibility of lower minimum horizontal stress in the upwards direction
Log of natural fault permeability (log(md))	$U[0,5]$	Ideally fault conductivity may be ascertained via injection tests. Value ranges based on fault throw to fault width correlation [26]
Natural fault porosity (unitless)	$U[0.05, 0.3]$	The Soultz geothermal site has measured porosities of up to 15% [27] in the fault zone. We increased this range to allow for more and less porous fault zones
Natural fault aperture (m)	$U[0.01, 1]$	McClure et al. [28] show that fault thickness varies from a few millimeter to several meters in other EGS sites. Image logs from the eastern flank of the Coso geothermal field identified faults ranging from sub-millimeter to fault zones about 30 cm thick [29]. We estimated the natural fault aperture to be around these measurements

the stimulated fractures are more highly controlled by the unknown natural parameters than by the stimulation process. Future work will include simulation of the stimulation process.

The values of the hydraulic fracture properties were taken from the literature. Table 3 lists the uncertain fracture properties and their range of values. These varying fracture parameters are illustrated in Fig. 4. There is a natural fault in this study, seen in Fig. 4(a). This natural fault also has unknown values of porosity, permeability and aperture. This study does not take into account the uncertainty of the natural fault's strike, dip and plunge, or address the possibility that there may be additional large faults nearby not intersected by existing wells. Future studies should include these factors.

The engineering decisions optimized in this study are shown in Table 4. These include the pressures used to inject water into the subsurface, the pumping power to extract the fluid from the subsurface, the distance between the fracture stages, the diameters of the wellbore and factors controlling the positioning of the wellbore.

The diameters of the wellbore can impact the flowrates of the injection to and production from the EGS. Pipe friction effects are inversely proportional to wellbore diameter and proportional to flow rate, as indicated in:

$$\left(\frac{dp}{dz}\right)_F = -f\rho_w\left(\frac{q}{\rho_w A}\right)^2/(2d) \tag{2}$$

where q is the mass flow rate, A is the cross-sectional area of the casing, ρ_w is the water density, d is the well diameter, and f is the Moody friction factor. Small wellbores can cause large friction losses due to their small diameters and given the high flowrates necessary in an EGS. Larger wellbores on the other hand carry with them a larger cost and therefore a financial penalty as described in the financial model section. This factor needs to be optimized.

The horizontal separation distance between the injector and producer is another engineering factor. There are advantages and disadvantages for locating the production well closer or further away from the injection well. Locating the producer closer to the injector well leads to a higher likelihood of intersecting stimulated hydraulic fractures and creating a high transmissivity flow connection. In addition, closer wellbores have higher flowrates given the same level of pressure differential. On the other hand, closer wellbores have less volumetric area from which thermal energy can be harvested between the wellbores. In addition, there is a higher chance of thermal short-circuiting since the cold fluid may have insufficient residence time to heat up as it flows from the injection to the production well. If the producer is positioned further away from the injection well, there is a risk of not intersecting a sufficient number of the hydraulic fractures. Yet, the EGS can recover a larger portion of thermal energy with larger separation between the injector and producer. Fig. 4 illustrates this parameter.

Another engineering parameter controlling the wellbore position is the “location of the injection well relative to the natural fault.” The area around the natural fault is hotter than the surrounding area since it carries hot fluid. The fault, however, may cause thermal short circuiting if it is too permeable. In such a case, it may be preferable to locate the wells to the east or to the west of the fault and avoid intersection with it. The location of the injection well with respect to the fault is normalized to the length of the wellbore. A value between zero and one indicates that the injection well intersects the fault at a normalized location along the wellbore length. For example, in Fig. 5(b) below, a fault position of 0.46 indicates that the fault intersects the wellbore in

Table 4
Engineering decision parameters.

Engineering decisions	Possible values	Additional information
Maximum well head pressure (kPa)	0–15,000	
Producer pump power (kW)	100–1500	Baker Hughes lists a 2000 HP geothermal pump (1491 kw)
Distance between the injection and production wells (m)	70–325	Well separation
Fracture spacing (m)	10;15;20;25	
Length of the well (m)	500–1000	
Producer well diameter Injector well diameter (m)	[0.103886, 0.115824, 0.128118, 0.155829, 0.166065, 0.180975, 0.205664, 0.226238, 0.254914, 0.279248, 0.318999, 0.385775, 0.446202]	Standard wellbore diameters
Location of the injection well relative to the natural fault	−0.5 to 1.5	The location of the injection well with respect to the fault normalized to the length of the wellbore

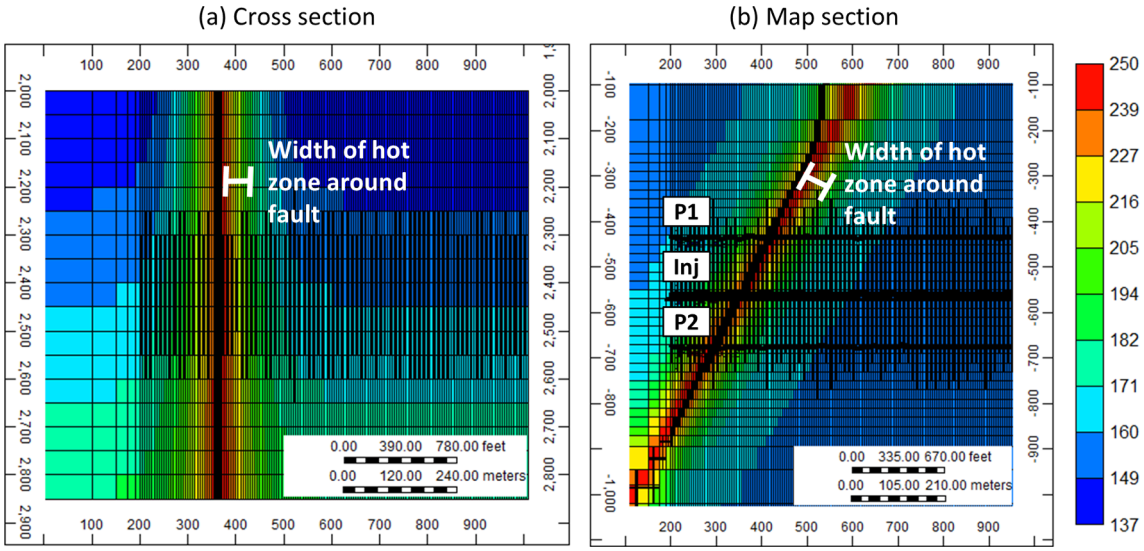

Fig. 3. Parameterization of the width of the hot zone around the fault in both (a) a cross-section and (b) map-section view. Modified from Pollack and Mukerji [42].

the middle the wellbore. Values between −0.5 and 0 indicate that the injection well is located to the west of the fault, and values between 1 and 1.5 indicate the injection well is to the east of the fault. Fig. 5 also illustrates the "well length" parameter.

2.2. Financial model for calculating net present value

For this paper, EGS performance metric is defined as the NPV over a twenty-year span of operations. The NPV takes into account the revenue from electricity generation, the parasitic losses of electricity to pumping, the costs of hydraulic fracturing, the wellbores, as well as the discount rate applied to the cash flow. It is calculated as follows:

$$NPV = \sum_{n=1}^{20} \frac{Net\ \ Electricity\ \ Sales}{(1 + Interest\ \ Rate)^n} - Initial\ \ Costs \tag{3}$$

The electricity generation is calculated as follows:

$$Sales_{electricity}\ \ (\$) = Electricity_{net}\ \ (\text{kw}\cdot\text{h})\cdot Price_{kW\cdot h} \tag{4}$$

$$Electricity_{net}\ \ (\text{kw}\cdot\text{h}) = Electricity_{gross}\ \ (\text{kw}\cdot\text{h}) - Electricity_{power\ pumps}\ \ (\text{kw}\cdot\text{h}) \tag{5}$$

$$Electricity_{gross}\ \ (\text{kw}\cdot\text{h}) = Mass\ Flow\ Rate\ \left(\frac{\text{kg}}{\text{s}}\right)\cdot \left(h_{inlet}\ \left(\frac{\text{kJ}}{\text{kg}}\right) - h_{outlet}\ \left(\frac{\text{kJ}}{\text{kg}}\right)\right)\cdot\eta_{plant}\cdot Hours \tag{6}$$

$$Electricity_{power\ \ pumps} = Electricity_{injection\ \ well\ \ pump} + Electricity_{production\ \ well\ \ pumps} \tag{7}$$

$$Electricity_{pump}\ \ (\text{kW}\cdot\text{h}) = Volumetric\ Flow\ Rate\ \left(\frac{\text{m}^3}{\text{s}}\right)\cdot \Delta Pressure_{across\ pump}\ \ (\text{kpa})\cdot Hours \tag{8}$$

where h_{inlet} and h_{outlet} are fluid enthalpy at the production wells and turbine outlet, respectively, $Electricity_{powerpumps}$ is the electricity necessary to power pumps to both inject fluid into the injection well and produce fluid from the production wells, and η_{plant} is the efficiency of the plant. In this equation, the main varying parameters are the fluid flow rate and the fluid temperature produced from the subsurface, which are taken from the hydro-thermal flow simulations. The plant efficiency declines with lowering temperatures, as shown in Fig. 6. The

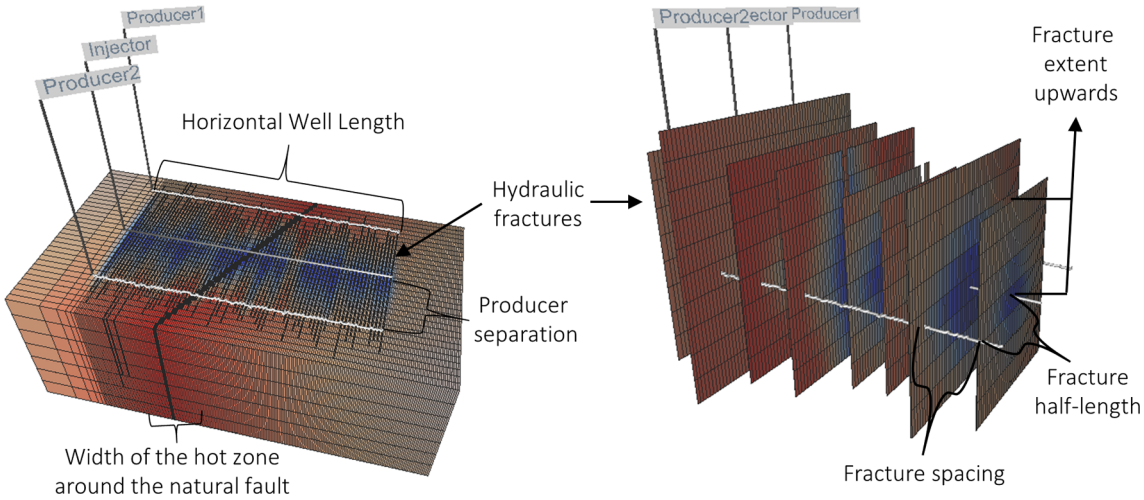

Fig. 4. Explanation of the parameterization of the enhanced geothermal system model. The left schematic shows the numerical block model. The right schematic shows only the thin elements representing the heterogeneous hydraulic fractures and the three wellbores. The colors indicate the temperature of the blocks. Cold water (blue) heats up (red) as it travels from the injection to the production wells.

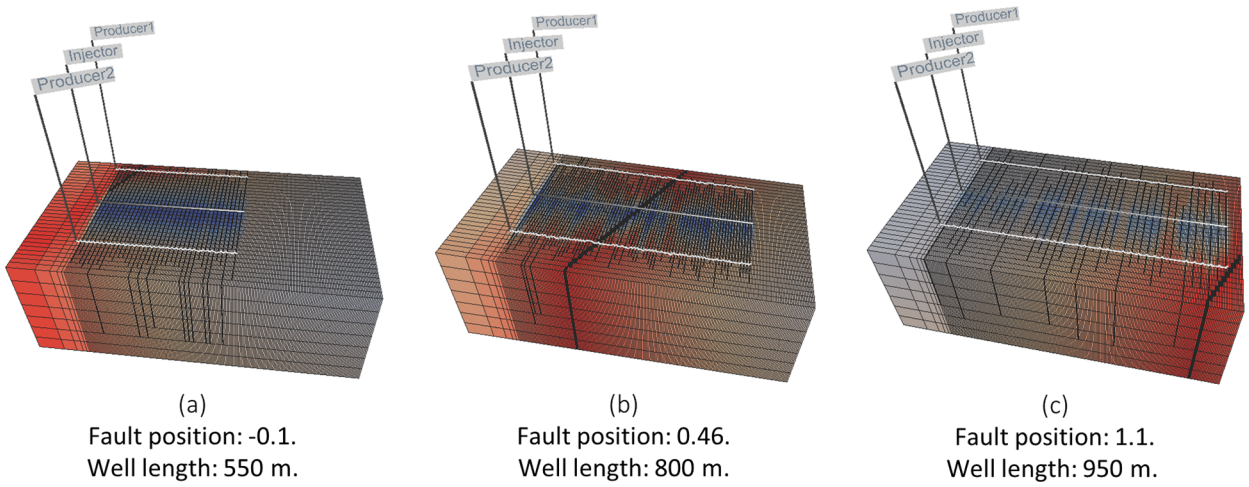

Fig. 5. Illustration of the parameters "location of the injection well with respect to the natural fault" and "well length." A value between −0.5 and 1 of fault position is an EGS with the injection well located to the east of the fault, as shown in (a). A value between 0 and 1, shown in (b), indicates that the fault is located along the length of the injection well. A value above 1, such as in (c), indicates the fault is to the east of the injection well. Different possible values of well length are indicated below the figures.

efficiency is initially around 0.12 and declines rapidly below 140 °C. The reinjection temperature is 76.5 °C.

The overall financial parameters for this model are shown in Table 5 below. The parameters include a sale price for the electricity, which is highly variable depending on the location of the geothermal facility. The cost for the different elements of the wellbore will affect the optimization results since these costs relate to several of the engineering parameters. For example, the cost of stimulation is a function of the number of hydraulic fractures in the model. The price of the wells is a function of the wellbore diameter, which is another factor that is optimized in this study. Many geothermal sites have spare capacity in their operating systems, and we are assuming that this geothermal facility is nearby an existing geothermal power plant. Therefore, we did not take into account the operating costs in this study, including the cost of using a binary unit to convert the hot fluid to electricity. Future work will include more rigorous estimates of the financial model parameters and the sensitivty of the optimization to these values.

3. Results

The following section includes analysis of the SM-Opt workflow and the MM-Opt workflow as well as a comparison of both workflows.

3.1. Results of SM-Opt workflow

For the SM-Opt workflow, 72 simulations (all with the same subsurface model but different choices of engineering decisions) were run using the PSO algorithm. As can be seen in Fig. 7, the PSO algorithm progressively improved the choice of engineering decisions to find the combination of engineering decisions that would yield the highest NPV.

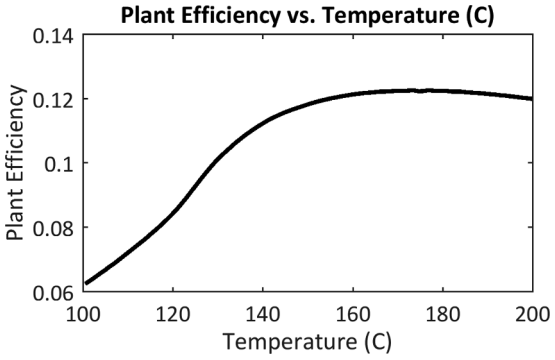

Fig. 6. Plant efficiency as a function of temperature. This shape of the curve is based on [35].

The optimal combination of parameters yielded an NPV of $32.7 million. The optimal engineering parameters were found to be:

- Length of the well: 950 m.
- Pump power of the producer wells: 917 kW.
- Distance between the injector and producers: 201 m.
- Maximum well head pressure of the injector well: 6897 kPa.
- Fracture spacing: 10 m.
- Producer wells' inner diameter: 0.17 m.
- Injector well's inner diameter: 0.28 m.
- Location of the well relative to the fault: 0. 67 (the well intersects the fault in the middle of the well length).

The SM-Opt workflow led to interesting results. The optimum well length is 950 m, while the possible range of well lengths was from 500 m to 1000 m. The length of the well adds cost to the project. This result shows that the additional flow rate possible from increasing the well length offsets the additional incurred costs for this constant earth model. This is a risky result of the SM-Opt workflow since it suggests a higher capital investment, which may only payoff for this specific earth model.

The optimal choices of values for the pumping power for the producer wells, the diameters of the wells, and the maximum well head pressure of the injector well lie in the middle of their possible ranges of values. This shows that the extra benefit yielded from increasing their values offsets the additional costs only up to a certain extent that needs to be optimized. While engineering models that do not take cost into account would recommend increasing wellbore sizes and pumping power to yield more energy, models that take the economic cost of these decisions into account show that such recommendations do not necessarily pay off. The economic models, however, add an extra sensitivity to the optimization study. A change in the cost of different operations, will change the optimal decisions.

The optimal fracture spacing for this reservoir model was found to be 10 m. This is the lowest value possible for this parameter. Though the high fracture density may cause thermal interaction between fractures, a lower fracture spacing translates into a larger number of fractures and a better thermal sweep of the resource. The added benefit from this additional thermal energy outweighed the cost of fracturing additional stages.

Table 5
Financial parameters.

Item	value	Source of information
Sale price per kW h ($)	0.076	This is the average price of electricity in recent geothermal PPA agreements [36]
Discount rate	0.15 for first two years and 0.07 for further years	Assumes a lower rate of interest after the plant is stable and operating
Cost per horizontal well length ($/m)	2600	Drilling in shale formation costs between $1200 and $1900 per lateral m [37]. Assuming drilling in igneous formation more expensive
Cost for stimulation ($)	250,000 * (number of stages)	The cost of stimulation is a function of the number of fracturing stages. A group of five fractures is considered a stage for this model. Shahkarami et al. [38] consider a fracture stage cost to be between $200,000 and $300,000
Cost for single vertical wellbore to 3000 m ($)	1,623,333–5,043,333	Depends on the wellbore diameter. Lowry et al. [39] reported costs of $2.6 million and $3.75 million for vertical wellbores to a depth of 3000 m with diameters of 8.50 in and 12.25 in respectively. These costs are expected costs for the near future (not present). Costs were interpolated and extrapolated for other wellbore diameter values used in this study

The optimal location of the wells relative to the fault was 0.67, such that the fault is located near the center of the well area. This is an interesting finding since the fault could be a cause of thermal short circuiting due to its higher permeability. On the other hand, the area near the fault is also hotter since it carries hotter fluid from deeper in the subsurface and has heated a substantial area around the fault over the years. This additional thermal energy offsets the possible thermal short circuiting for this scenario.

Fig. 8 below shows the simulated time series of the temperature, mass rate and net power generation over time of the reservoir model given the different operating decisions. The simulation of the optimal engineering values is shown in red. The optimal scenario has high fluid temperature and modest temperature drawdown, a high flow rate and a high level of power generation. The scenario with the optimal decisions, though, does not yield the highest temperatures or flow rates. This relates to finding a balance between parameters. Systems that have low temperature drawdown tend to have low flow rates, and thus it is not necessarily ideal to have the lowest temperature drawdown. Systems that have high flow rates, on the other hand, have high temperature drawdowns, which is also not ideal. In addition, systems with high power generation may have higher patristic loads due to high pumping levels or higher costs from larger wellbores or longer wells. Therefore, optimization does not necessarily lead to an EGS with the highest generation capacity.

3.2. Results of MM-Opt workflow

For the MM-Opt workflow, 1000 uncertain parameter combinations were sampled and used to build numerical models. The hydrothermal simulation of the models for a twenty-year period from 2019 to 2039 yielded curves of the temperature and mass flow rate of the produced fluid, shown in Fig. 9(b). The flow rate and temperature curves were used to calculate the power generation over time and NPV, shown by the temporal curves and histogram in Fig. 9(c), respectively. The realizations were clustered into high and low energy capacity groups using the K-means clustering algorithm [40]. The high and low energy capacity groups are indicated by the red and blue colors, respectively, in Fig. 9. Overall, the models show a wide range of NPV from a P10 of $-17 M to a P90 of $7 M. The large variability in power generation highlights the importance of finding the factors that most influence an EGS and further researching them to ensure high capacity systems.

3.2.1. Sensitivity analysis

The classified models were used to build cumulative density functions (CDFs) of the model parameters conditioned on the high and low capacity classes. For example, the CDFs of the mean fracture half-length and mean fracture aperture are shown in Fig. 10(a). The high capacity CDFs in pink, for both parameters, are separated from the prior CDFs in black, and show that higher values of fracture half-length and fracture aperture contribute to higher capacity models. The CDFs of each parameter were used to compute the most sensitive parameters, shown in the Pareto plot in Fig. 10(b), using the Distance Based Generalized Sensitivity Analysis algorithm [41]. There are fifteen parameters that were deemed to be highly influential, which can be seen as having a significance level above 95 in the Pareto plot in Fig. 10(b).

The most influential parameter is the mean fracture aperture. Models that had mean fracture apertures with high values were found to generate more electricity. Large fracture apertures lead to higher flow rates and additional generated heat. The second most influential parameter is the mean fracture half-length, which directly controls the size of the stimulated reservoir that can be mined for thermal energy. Larger fractures allow for longer heat exchange or residence time as the

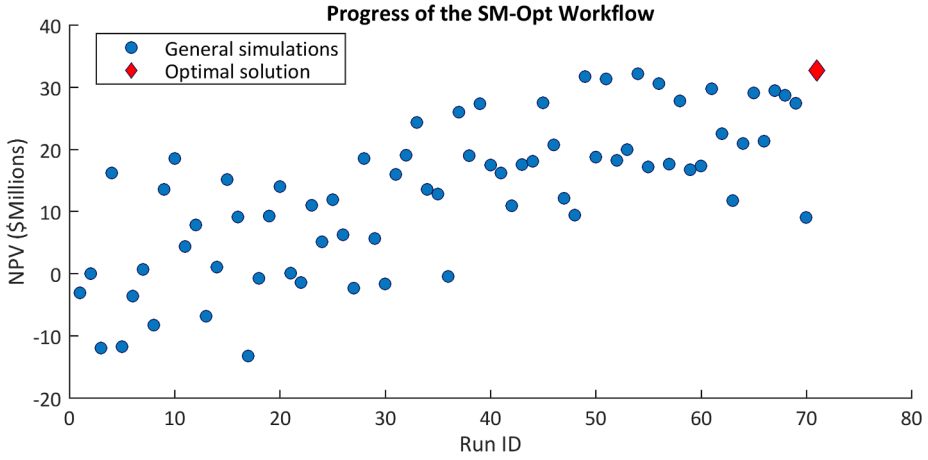

Fig. 7. Progress of the SM-Opt workflow using the PSO algorithm to optimize the engineering decisions for a single reservoir model.

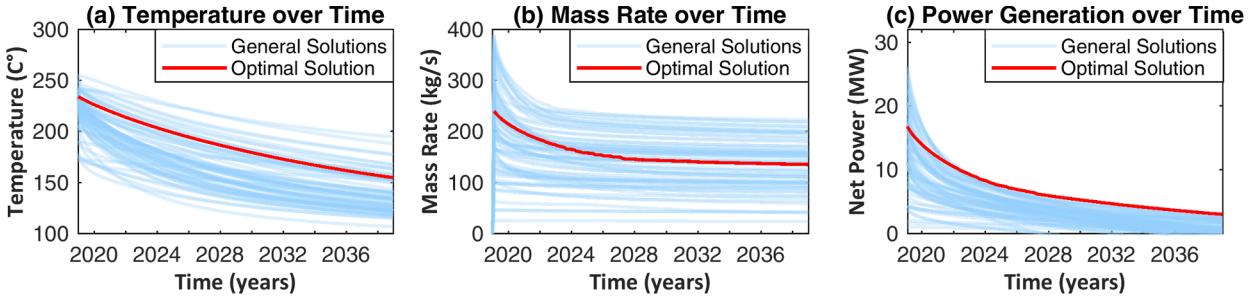

Fig. 8. The (a) temperature, (b) mass rate and (c) net power generation over time of the investigated reservoir model given different operating decisions. The simulation with the optimal operating decisions is marked by a red line.

water flows between the injector and producer wells.

While both fracture half-length and fracture aperture are controlled by the hydraulic fracturing process, it is difficult to control such values due to the complexity of the subsurface environment and fracturing process. In this analysis, the hydraulic fracture properties were set to be random variables for each realization since it is difficult to predict hydraulic fracture properties prior to experimentation in the particular subsurface environment. Since the mean fracture half-length and mean fracture aperture are the top influential parameters on the NPV of an EGS, there is further incentive to investigate controlling such parameters via use of fracturing fluids and proppant.

The third sensitive parameter is the width of the hot zone around the fault. Often, there is just a single exploration well to determine the temperature distribution in the subsurface, and it is unclear how far the elevated temperature zone extends spatially. This is another subsurface parameter that is often unknown and which highly influences EGS success. The seventh (natural fault permeability), eleventh (matrix permeability), twelfth (matrix heat capacity) and thirteenth (natural fault porosity) sensitive parameters are also natural subsurface properties that cannot be changed but are impactful. Natural faults with low to medium permeability and high porosity contribute to higher NPV. A fault with high permeability can lead to thermal breakthrough, lower production temperatures, and therefore lower profit. Higher matrix permeability and matrix heat capacity lead to higher NPV.

While the first two sensitive parameters are partially beyond engineering control, the fourth, fifth, sixth, eighth, ninth, tenth and fourteenth sensitive parameters can be controlled. These engineering decisions are discussed in further detail in the following section. All of the other parameters had a lower influence on the NPV as compared to the above-mentioned parameters.

3.2.2. *Optimal engineering decisions*

We constructed probability distribution functions (PDFs) of the NPVs conditioned on the different engineering decisions to assess the optimal engineering choices. Fig. 11(a) shows the PDF of NPVs separated into the realizations with fracture spacing of 10, 15, 20 and 25 m. The vertical lines on the bottom of the graph show the median NPV values for each level of fracture spacing, indicated by matching colors. The PDFs of realizations with a fracture spacings of 10 and 15 have the highest median NPV, with a fracture spacing of 10 m being slightly higher. A lower fracture spacing increases the number of fractures and the overall system transmissivity but is also more expensive as more fracture stages are necessary (see financial model). Similar to SM-Opt, the MM-Opt workflow results suggest that the additional transmissivity offsets the cost of additional fracturing operations at the 10–15 m level.

Fig. 11(b) shows the PDFs of NPVs of the distance between injector and producers. Realizations with a producer distance between 155 and 240 m (red line) have the highest median NPV. The hydraulic fractures

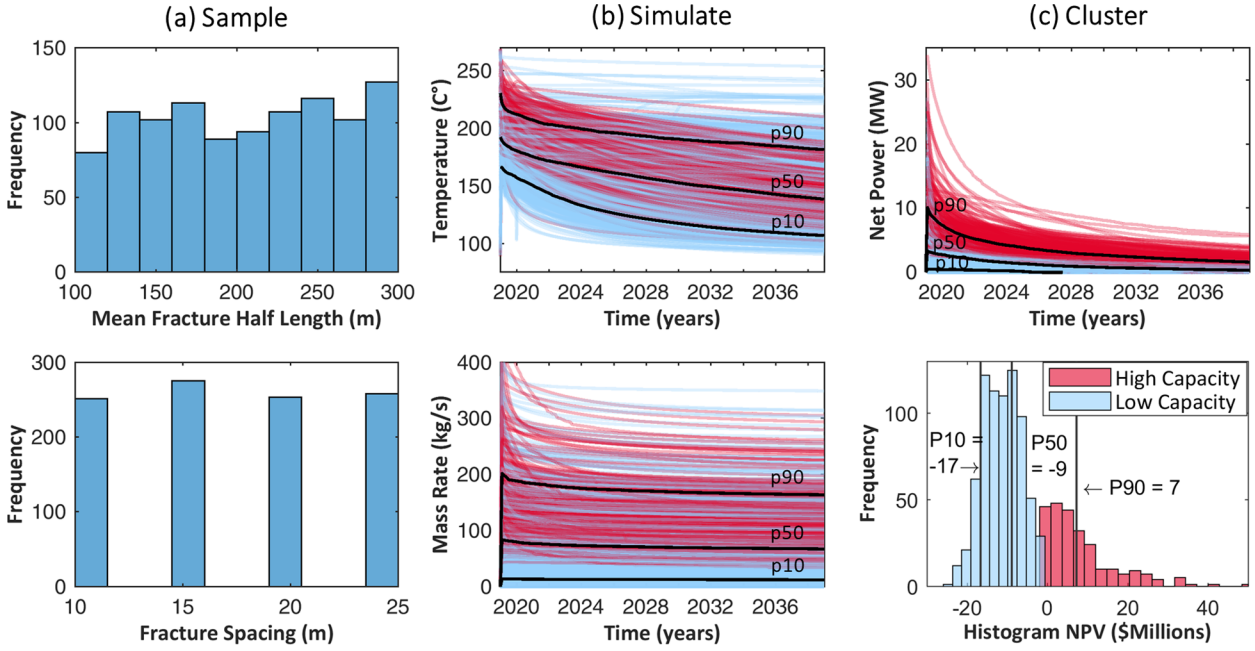

Fig. 9. (a) Sampled values of the mean fracture half-length and fracture spacing parameters used in the realizations. (b) Simulated mass rate, temperature, and (c-top) energy generation over time of the stochastically generated models. (c-bottom) A histogram of the NPVs of the realizations. The colors red and blue indicate high and low capacity models, respectively.

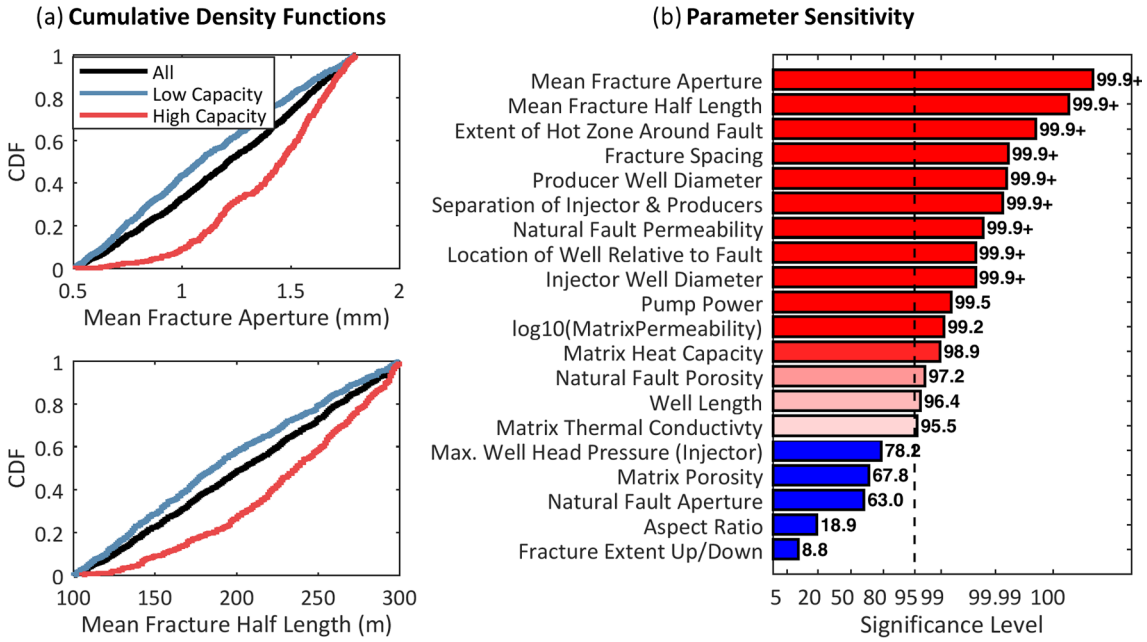

Fig. 10. (a) The cumulative distribution function (CDF) plots of the (top) mean fracture half-length and (bottom) mean fracture aperture of the model realizations. The curves indicate the CDFs of the high capacity cluster, low capacity cluster, and total prior distribution, in pink, light blue and black, respectively. (b) Pareto plot showing the relative ranking of parameter sensitivities.

in the realizations had mean half lengths varying between 100 and 300 m. The results show that a robust EGS should have the producers located approximately in the middle of the range of possible lengths. The choice of having a larger separation (green line) leads to both potentially higher NPV values (when the hydraulic fractures are actually longer and reach a further positioned production well) and potentially lower NPV values (when the producer is located too far from the injector and does not intersect any fractures).

The PDFs of NPVs separated into three levels of production well pumping power are shown in Fig. 12(a). Low and medium levels of pumping power show only a slight improvement to the NPV over higher pumping power. The pumping power adds a parasitic loss to the EGS. For this study, the additional flow rate from pumping does not compensate for the additional pumping cost.

Fig. 12(b) shows the PDFs of NPVs separated into three levels of injector well head pressure (WHP). Realizations with a high injector well head pressure (the green line in Fig. 12(b)) shows a slightly higher NPV, indicating that the high injection rates increase the NPV even though they are associated with an increase in parasitic pumping power.

The PDFs of the NPV separated into three levels of well length are shown in Fig. 13(a). There is little difference in the median NPV regardless of the well length, with only slight preference for short to medium length horizontal wellbore sections. The additional energy recovery from increasing the well length and generating additional electricity is offset by the increased cost of a longer well.

One of the most sensitive decisions is the location of the well relative to the natural fault. It is clearly optimal to intersect the natural fault (a range of values 0–1 leads to an intersection of the natural fault, with the value of this parameter indicating the location of intersection relative to the well length). Even though the fault may cause thermal short circuiting, the additional thermal energy gained from locating the EGS in the hot rock surrounding the natural fault overwhelmingly compensates for the risk of thermal short circuiting.

The PDFs of the NPV separated into two levels of well diameter are shown in Fig. 14(a) for the production wells and Fig. 14(b) for the injection well. Smaller wellbore diameters for both the production and injection wells lead to higher NPV. A larger well diameter is more costly and a smaller well diameter has higher friction and therefore energy losses. The cost savings from using smaller well diameters outweighs the energy savings of using large wellbores.

The results presented above indicate that an EGS with a fracture spacing of 10 or 15 m, smaller well diameters, a distance between 155 and 240 m between the injection and production wells, and which intersects the natural fault will yield higher NPVs. Fig. 15 below shows

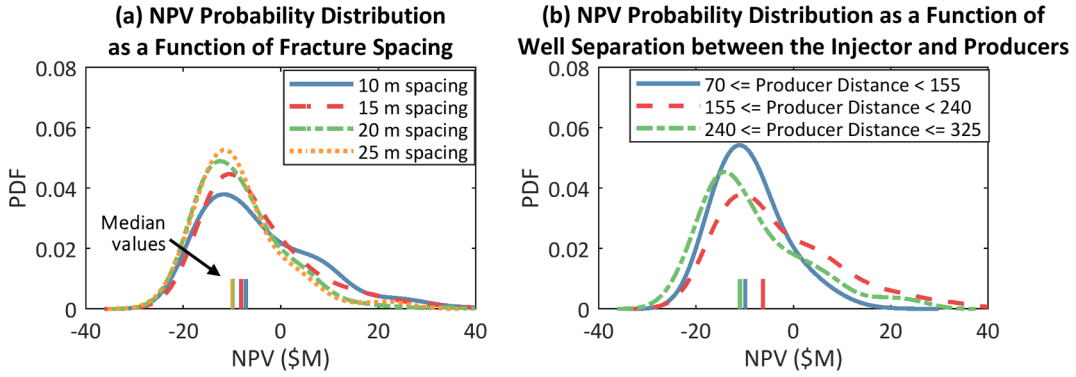

Fig. 11. The histogram of NPVs of the stochastically generated EGS models separated into different levels of (a) fracture spacing and (b) well separation. The vertical lines on the bottom axis indicate the median NPV of each group.

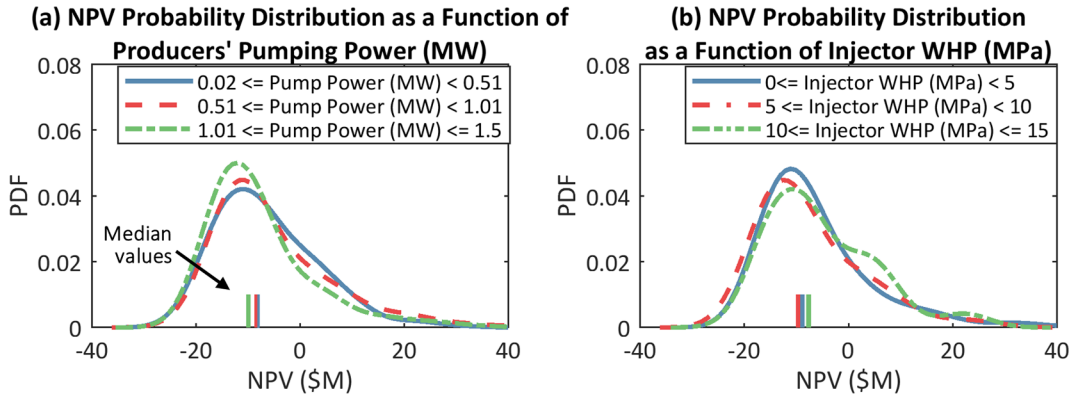

Fig. 12. The histogram of NPVs of the stochastically generated EGS models separated into different levels of (a) production wells' pumping power and (b) the Well Head Pressure (WHP) of the injection well. The vertical lines on the bottom axis indicate the median NPV of each group.

the PDF of NPVs of all models in blue and the PDF of NPVs of the models with optimized engineering decisions. The optimized realization have a median NPV of $11 million and a standard deviation of $15 million. There is a 20 million dollar difference in the median NPV values between the group of realizations with the optimized engineering decisions versus the general prior realizations. There is a large uncertainty, though, in NPV for both the prior and optimized scenarios. This is because the uncertain and random subsurface parameters have the most influence on the NPV of the EGS given this study's model parameterization and uncertainty ranges. In addition, both PDF curves are not completely symmetric and unimodal, likely due to the presence of non-linear processes in enhanced geothermal systems.

3.3. Comparison between the optimization workflows

Two varying workflows have been used to optimize the EGS: SM-Opt and MM-Opt. SM-Opt keeps the reservoir model constant and optimizes the engineering parameters. The optimal engineering parameters are those that lead to the highest NPV. MM-Opt varies the earth parameters of the reservoir model within the ranges of the parameters' possible values, while also varying the engineering parameters. The optimal engineering parameters are those that have the highest median NPV.

The optimal parameters for the two methods are shown in Table 6 below. While the SM-Opt methodology gives a single parameter, the MM-Opt gives a range of optimal values. MM-Opt using the Monte Carlo algorithm necessitates a large number of simulations for each range of engineering decisions in order to account for the changing earth models. With a larger number of simulations than used in this study, the Monte Carlo method can be used to ascertain more precise ranges of optimal solutions.

For several of the engineering parameters, the MM-Opt indicated that there is no preferred value for those engineering parameters. This carries the additional useful information that the EGS is not sensitive to those parameters.

The results in Table 6 indicate that for this problem setup the optimal engineering decisions for both methods are similar. In general, the SM-Opt identified the decisions that the MM-Opt workflow identified as most robust in the face of subsurface uncertainty. A difference is present in the choice of well head pressure. In addition, for two of the parameters: the horizontal length of the well and pump power, there is no indicated preference given by the MM-Opt workflow.

Fig. 16 shows the horizontal well length versus the NPV for the simulations of the SM-Opt workflow and MM-Opt workflow. The optimal well length using SM-Opt is 950 m, as shown in the scatter plot of Fig. 16(a). On the other hand, for the MM-Opt simulations shown in Fig. 16(b), there is little correlation between well length and NPV. In fact, the median NPV of realizations with well length above 833 m is slightly lower as compared to horizontal well lengths less than 833 m. Given the similar median NPV values for the possible well lengths, the optimal choice based on the MM-Opt workflow would be to have a shorter wellbore and therefore less initial financial investment.

Fig. 17 shows the NPVs for different fracture spacing criteria for simulations from the SM-Opt workflow (Fig. 17(a)) and the MM-Opt Workflow (Fig. 17(b)). The SM-Opt workflow shows a clear increase in NPV as the fracture spacing is decreased. For the MM-Opt workflow, the median NPV also increases as the fracture spacing is decreased. The difference, however, between a fracture spacing of 10 and 15 m is minimal. For the SM-Opt model, there was one specific set of values for fracture aperture and fracture length. For these specific set of values, additional fractures yielded sufficient energy generation to offset the additional cost of fracturing. On the other hand, in the MM-Opt workflow, the fracture spacing is not the most sensitive parameter. Once more, an operator may decide based on this data that it is not

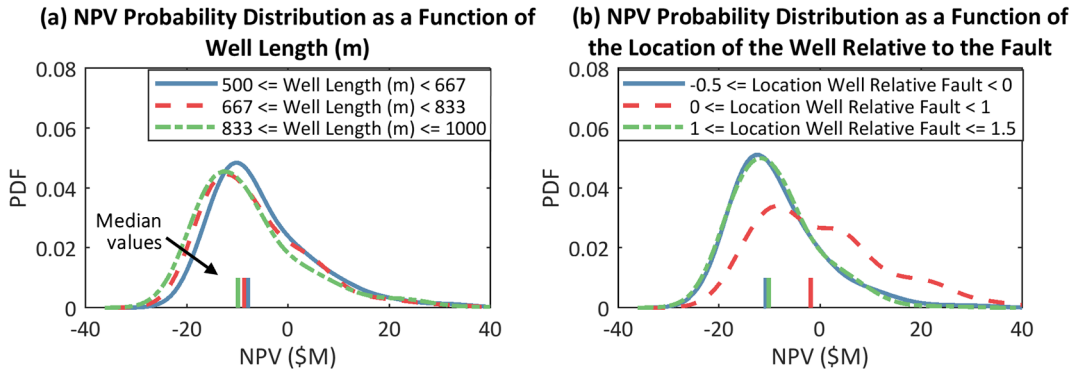

Fig. 13. The histogram of NPVs of the stochastically generated EGS models separated into different levels of (a) well length and (b) the location of the well relative to the fault. The vertical lines on the bottom axis indicate the median NPV of each group.

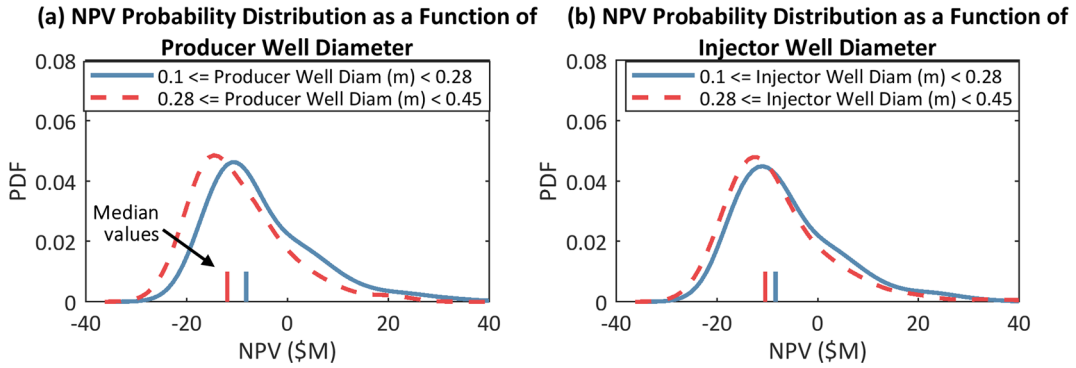

Fig. 14. The histogram of NPVs of the stochastically generated EGS models separated into different levels of (a) production wells' and (b) injection well's inner diameter. The vertical lines on the bottom axis indicate the median NPV of each group.

crucial to pay additional money for more closely spaced hydraulic fractures.

Another important observation in this graph is that SM-Opt generated an optimum NPV of $32.7 million for a fracture spacing of 10 m, pointed to by the gray arrow in Fig. 17. On the other hand, the MM-Opt led to a median value of $-6.3 million for a fracture spacing of 10 m. The MM-Opt is not a worse optimization tool because of this lower value. SM-Opt outputs a single optimal solution that is the highest value achieved during the optimization process. The highest value in the MM-Opt is $53.5 shown as the red outlier above the box plot of fracture spacing of 10 m in Fig. 17(b). The optimal solution SM-Opt is beyond the 75th quantile of the MM-Opt, with the location indicated by the gray arrow in Fig. 17(b). The representative model used in the SM-Opt was created by taking the mean values for each parameter. It is possible that this is a particularly good combination of earth parameters, but in reality, it is one of many possible combinations.

Table 6
Comparison of optimal engineering parameters for the two workflows: optimization given a single reservoir model (SM-Opt) and optimization given reservoir model uncertainty (MM-Opt).

Engineering parameter	SM-Opt	MM-Opt
Length of the well (m)	950	No preference
Pump power of the producer wells (kW)	917	No preference
Distance between the injector and producers (m)	201	Preference for a distance between 155 and 240
Injector maximum well head pressure (MPa)	6.9	Above 10 MPa
Fracture spacing (m)	10	10 or 15
Producer wells inner diameter (m)	0.17	Less than 0.28
Injector well inner diameter (m)	0.28	Less than 0.28
Location of well relative to the fault (unitless ratio)	0.67	Between 0 and 1

4. Application of MM-Opt to real sites

This methodology could be used, for example, at the US Department of Energy Frontier Observatory for Research in Geothermal Energy (FORGE) site in Utah, which will be commencing construction of an experimental enhanced geothermal system in 2020. They have not yet drilled their main 'injection well. They need to decide where to place the well, what diameter to make the well, how deep to make the well, and what should be the horizontal length of the wellbore. This paper shows that considering subsurface uncertainty may influence operational decisions. Therefore, the FORGE team could perform the same workflow for MM-Opt as shown in this paper:

I. assess the ranges of uncertainty of the subsurface properties,
II. create an ensemble of reservoir models that are possible given the subsurface uncertainty, and
III. perform an optimization on this ensemble of reservoir models.

This study investigates the process of decision making under uncertainty for an EGS facility employing multi-stage hydraulic fracturing in a cased horizontal wellbore. Unfortunately, this use of shale gas technology has not yet been tested in a geothermal context and therefore no data from a real site can be incorporated into this study. This study gives insight for future construction of enhanced geothermal facilities. This methodology is crucial for such sites since no matter how

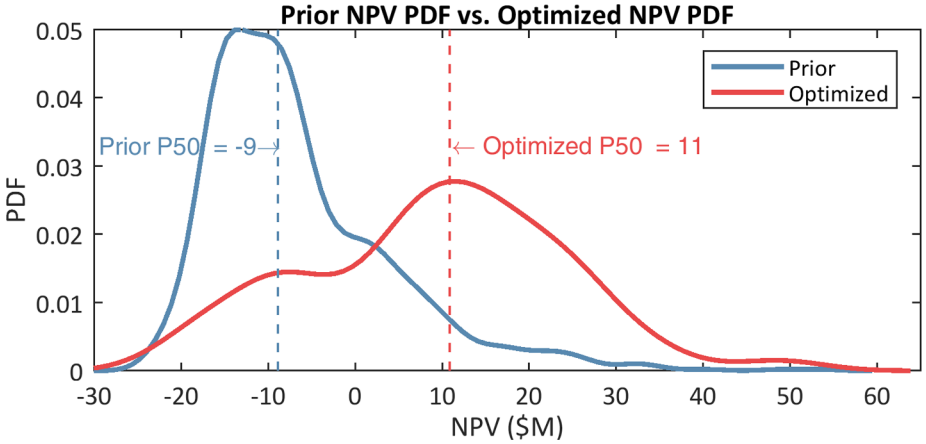

Fig. 15. PDF of the NPVs of all the stochastically generated EGS models in blue relative to the PDF of the NPVs of EGS models with optimized engineering decisions in red.

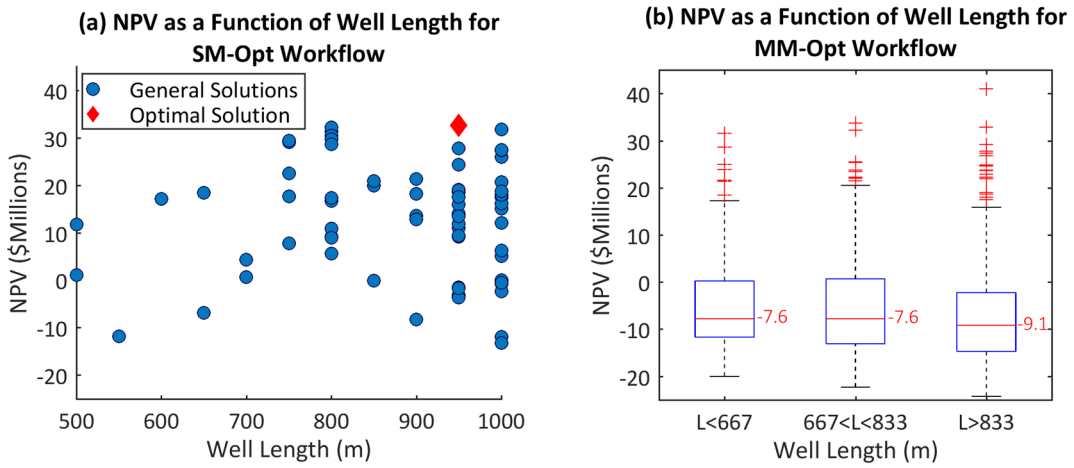

Fig. 16. Scatter plot of NPV versus horizontal well length for the simulations of the (a) SM-Opt workflow. (b) A box plot of NPV versus horizontal well length for the realizations from the MM-Opt workflow. The central mark indicates the median, and the bottom and top edges of the box indicate the 25th and 75th percentiles, respectively.

much exploration is done, there will always be uncertainty about the subsurface. One way of tackling this uncertainty is ignoring it by creating one single model, or SM-Opt. In this study, we present another option, MM-Opt, and showed that it can lead to more robust solutions that will garner higher expected revenue as well as better risk understanding.

5. Conclusions and future work

This study investigated two workflows for optimizing engineering decisions for an EGS: a SM-Opt workflow with a single deterministic earth model and a MM-Opt workflow with an ensemble of reservoir models. This study found that the SM-Opt led to an optimum NPV with the following values: well length of 950 m, pumping power of 917 kW for the producer wells, a distance between the production wells and injection well of 210 m, a maximum well head pressure of 6.9 MPa, a fracture spacing of 10 m, an inner diameter of 0.17 m for the production wells, an inner diameter of 0.28 m for the injection well, and positioning the EGS such that it intersects the fault.

The MM-Opt workflow led to optimum NPV values with a fracture spacing of 10–15 m, well diameters less than 0.28 m, an EGS system that intersects the natural fault, a high injection pressure, and a distance of 144 to 240 m between the injection and production wells. There were no preferred optimum values for the pumping power of the production wells, and length of the well, as these were insensitive parameters given the range of subsurface uncertainty.

The optimal decisions are similar for both optimization methods, besides for the parameters that are not influential in the MM-Opt workflow. For the insensitive parameters, an EGS operator may choose the less costly engineering options in order to lower upfront investment. This additional information regarding the sensitivity of the parameters can thus impact the chosen engineering decisions.

Overall, the SM-Opt workflow suggested more optimistic results, yielding an optimum NPV of $32.7 million. On the other hand, the MM-Opt yielded a median NPV for the optimized engineering parameters of $11 million and large uncertainty margins. When the subsurface properties are known, as is assumed in SM-Opt, optimization can yield high values that overestimate EGS productivity and are optimal for one specific scenario. While the MM-Opt median value is unsatisfactorily low, it highlights the need to either investigate engineering methods that are more robust to uncertain earth parameters or better methods to reduce subsurface uncertainty. Having a realistic view of expected NPV given the subsurface uncertainty can push for more subsurface assessment and engineering analysis prior to making engineering decisions.

In addition, this work has found that EGS productivity is most impacted by variables that were considered outside of the scope of engineering: the hydraulic fracture-related parameters of mean fracture length and mean fracture aperture. These finding highlight the relative

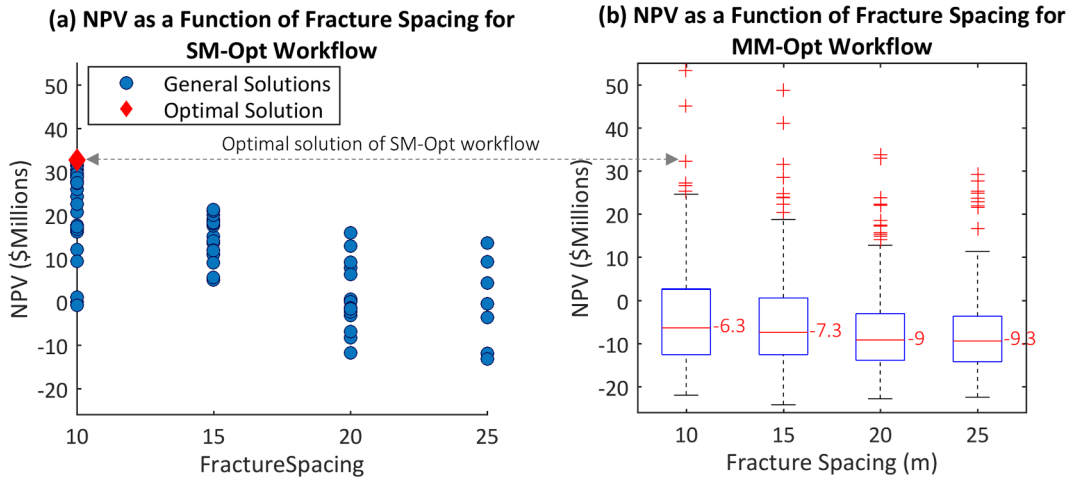

Fig. 17. Scatter plot of NPV versus fracture spacing for the simulations of the (a) SM-Opt workflow. (b) A box plot of NPV versus fracture spacing for the realizations from the MM-Opt workflow. The central mark indicates the median, and the bottom and top edges of the box indicate the 25th and 75th percentiles, respectively.

importance of further researching hydraulic fracturing technology to create larger hydraulic fractures with greater apertures. Future work will include: simulating hydraulic fracture propagation in the presence of natural fractures and one or more natural faults, calculating important geomechanical effects such as thermal stresses, and integrating field data.

Acknowledgements

This material is based upon work supported by the National Science Foundation (NSF) Graduate Research Fellowship Program under Grant No. 1656518, as well as sponsors of Stanford Center for Earth Resources Forecasting. We acknowledge Computer Modeling Group for the licenses of STARS and CMOST, as well as the use of the CMG internal cloud. Special thanks to Jim Erdle, Kiran K. Venepalli, and Richard Li at CMG for their assistance. We acknowledge Emerson/Paradigm for providing a license of SKUA.

References

[1] Pachauri RK, Allen MR, Barros VR, Broome J, Cramer W, Christ R, et al. Synthesis report: summary for policymakers. Contrib work groups I, II III to fifth assess rep intergov panel clim chang 2014;2014:31. https://doi.org/10.1017/CBO9781107415324.
[2] U.S. Energy Information Administration. September 2016 monthly energy review; 2016. doi:DOE/EIA-0035(2011/02).
[3] Tester JW, Anderson BJ, Batchelor AS, Blackwell DD, DiPippo R, Drake EM. The future of geothermal energy; 2006.
[4] Riffault J, Dempsey D, Karra S, Archer R. Microseismicity cloud can be substantially larger than the associated stimulated fracture volume: the case of the paralana enhanced geothermal system. J Geophys Res Solid Earth 2018;123:6845–70. https://doi.org/10.1029/2017JB015299.
[5] Li T, Shiozawa S, McClure MW. Thermal breakthrough calculations to optimize design of a multiple-stage Enhanced Geothermal System. Geothermics 2016. https://doi.org/10.1016/j.geothermics.2016.06.015.
[6] Asai P, Panja P, McLennan J, Moore J. Performance evaluation of enhanced geothermal system (EGS): surrogate models, sensitivity study and ranking key parameters. Renew Energy 2018;122:184–95. https://doi.org/10.1016/j.renene.2018.01.098.
[7] Song X, Shi Y, Li G, Yang R, Wang G, Zheng R, et al. Lyu Z Numerical simulation of heat extraction performance in enhanced geothermal system with multilateral wells. Appl Energy 2018;218:325–37. https://doi.org/10.1016/j.apenergy.2018.02.172.
[8] Doe T, Mclaren R. Discrete fracture network analysis of controlling factors for EGS performance. Proc Geotherm Reserv Eng Stanford Univ 2016:1–10.
[9] Guo B, Fu P, Hao Y, Peters CA, Carrigan CR. Geothermics Thermal drawdown-induced flow channeling in a single fracture in EGS. Geothermics 2016;61:46–62. https://doi.org/10.1016/j.geothermics.2016.01.004.
[10] Hu X, Tutuncu A, Eustes A, Augustine C. Optimizing for large planar fractures in multistage horizontal wells in enhanced geothermal systems using a coupled fluid and geomechanics simulator. Trans - Geotherm Resour Counc 2016;40:325–34.
[11] Hofmann H, Babadagli T, Zimmermann G. Hot water generation for oil sands processing from enhanced geothermal systems: process simulation for different hydraulic fracturing scenarios. Appl Energy 2014;113:524–47. https://doi.org/10.1016/j.apenergy.2013.07.060.
[12] Mottaghy D, Pechnig R, Vogt C. The geothermal project Den Haag: 3D numerical models for temperature prediction and reservoir simulation. Geothermics 2011;40:199–210. https://doi.org/10.1016/j.geothermics.2011.07.001.
[13] Vogt C, Kosack C, Marquart G. Stochastic inversion of the tracer experiment of the enhanced geothermal system demonstration reservoir in Soultz-sous-Forêts - Revealing pathways and estimating permeability distribution. Geothermics 2012;42:1–12. https://doi.org/10.1016/j.geothermics.2011.11.001.
[14] Tompson A, Mellors RJ, Ramirez A, Chen M, Dyer K, Yang X, et al. Stochastic joint inversion of a geothermal prospect. Geotherm resour counc annu meet. 2013. p. 510–7.
[15] Mellors RJ, Tompson A, Dyer K, Yang X, Chen M, Wagoner J. Stochastic joint inversion modeling algorithm of geothermal prospects. Proceedings, thirty-ninth work geotherm reserv eng. 2014. p. 1–7.
[16] Cui T, Fox C, Sullivan MJO, O'Sullivan MJ. Bayesian calibration of a large-scale geothermal reservoir model by a new adaptive delayed acceptance metropolis Hastings algorithm. Water Resour Res 2011;47.. https://doi.org/10.1029/2010WR010352.
[17] Vogt C, Marquart G, Kosack C, Wolf A, Clauser C. Estimating the permeability distribution and its uncertainty at the EGS demonstration reservoir Soultz-sous-Forts using the ensemble Kalman filter. Water Resour Res 2012;48:1–15. https://doi.org/10.1029/2011WR011673.
[18] Marquart G, Vogt C, Klein C, Widera A. Estimation of geothermal reservoir properties using the ensemble Kalman filter. Energy Proc 2013;40:117–26. https://doi.org/10.1016/j.egypro.2013.08.015.
[19] Onur M, Palabiyik Y. Nonlinear parameter estimation based on history matching of temperature measurements for single-phase liquid-water geothermal reservoirs. World geotherm congr 2015. 2015. p. 19–25.
[20] Kennedy J, Eberhart R. Particle swarm optimization. Proc. ICNN'95 - int conf neural networks, vol. 4. IEEE; 1995. p. 1942–8. https://doi.org/10.1109/ICNN.1995.488968.
[21] Blankenship D, Blake K, Calvin W, DeOreo S, Faulds JE, Glen JMG, et al. Frontier observatory for research in geothermal energy: phase 1 topical report west flank of Coso, CA; 2016, p. 265.
[22] Schon JH. Physical properties of rocks. Handb pet explor prod. Amsterdam: Elsevier; 2011. p. 781588.
[23] Cermak V, Rybach L. Thermal conductivity and specific heat of minerals and rocks. Landolt-Börnstein, New Ser. Gr. V, Geophys. Sp. Res.; 1982. https://doi.org/10.1007/10201894_62.
[24] Reinicke A. Mechanical and hydraulic aspects of rock-proppant systems laboratory experiments and modelling approaches; 2009. https://doi.org/10.2312/GFZ.b103-11098.
[25] Zimmermann G, Moeck I, Blöcher G. Cyclic waterfrac stimulation to develop an Enhanced Geothermal System (EGS)-Conceptual design and experimental results. Geothermics 2010;39:59–69. https://doi.org/10.1016/j.geothermics.2009.10.003.
[26] Manzocchi T, Walsh JJ, Nell P, Yielding G. Fault transmissibility multipliers for flow simulation models. Pet Geosci 1999;5:53–63. https://doi.org/10.1144/petgeo.5.1.53.
[27] Géraud Y, Rosener M, Surma F, Place J, Le Garzic É, Diraison M. Physical properties of fault zones within a granite body: example of the Soultz-sous-Forêts geothermal site. Comptes Rendus - Geosci 2010;342:566–74. https://doi.org/10.1016/j.crte.2010.02.002.
[28] McClure MW, Horne RN. An investigation of stimulation mechanisms in Enhanced Geothermal Systems. Int J Rock Mech Min Sci 2014;72:242–60. https://doi.org/10.1016/j.ijrmms.2014.07.011.
[29] Davatzes NC, Hickman SH. Stress, fracture, and fluid-flow analysis using acoustic and electrical image logs in hot fractured granites of the Coso Geothermal Field, California, U.S.A. AAPG mem 92 dipm boreh image log technol 2010. p. 259–93. https://doi.org/10.1306/13181288M923134.
[30] Computer Modeling Group Ltd. User's guide STARS advanced process and thermal reservoir simulator; 2017.
[31] Zhou Q, Oldenburg CM, Rutqvist J. Revisiting the analytical solutions of heat transport in fractured reservoirs using a generalized multirate memory function. Water Resour Res 2019. https://doi.org/10.1029/2018wr024150.
[32] Xu R, Zhang L, Zhang F, Jiang P. A review on heat transfer and energy conversion in the enhanced geothermal systems with water/CO2 as working fluid. Int J Energy Res 2015;39.. https://doi.org/10.1002/er.
[33] Jaeger JC, Carslaw HS. Conduction of heat in solids. 2nd ed. Oxford: Oxford Clarendon Press; 1959. p. 255. https://doi.org/10.1063/1.3057871.
[34] McKenna JR, Blackwell DD. Numerical modeling of transient basin and range extensional geothermal systems. Geothermics 2004;33:457–76. https://doi.org/10.1016/j.geothermics.2003.10.001.
[35] Lukawski MZ, Dipippo R, Tester JW. Molecular property methods for assessing efficiency of organic Rankine cycles. Energy 2018;142:108–20. https://doi.org/10.1016/j.energy.2017.09.140.
[36] Hernandez K, Richard C, Nathwani J. Estimating project LCOE – an analysis of geothermal PPA data. Proc 41st work geotherm reserv eng. 2016. p. 1–8.
[37] Fullenbaum R., Smith C, Rao M, Xiao J, Adams S, Fontaine R. Trends in US oil and natural gas upstream costs; 2016. https://doi.org/10.3415/VCOT-11-11-0166.
[38] Shahkarami A, Wang G, Belyadi H. Horizontal well spacing and hydraulic fracturing design optimization: a case study on utica-point pleasant shale play. Unconv resour technol conf. 2016. p. 1–3. doi:10.15530-urtec-2016-2459851.
[39] Lowry TS, Finger JT, Carrigan CR, Kennedy MB, Corbett TF, Doughty CA, et al. Reservoir maintenance and development task report for the DOE geothermal technologies office geovision study; 2017.
[40] Macqueen J. Some methods for classification and analysis of multivariate observations. Proc fifth berkeley symp math stat probab, vol. 1. 1967. p. 281–97. doi:citeulike-article-id:6083430.
[41] Scheidt C, Li L, Caers J. Quantifying uncertainty in subsurface systems. Hoboken, NJ, USA: John Wiley & Sons, Inc.; 2018. doi:10.1029/2011GM001187.Cited.
[42] Pollack A, Mukerji T. Optimization of Enhanced Geothermal Systems under Geological and Reservoir Stimulation Uncertainty. GRC Trans 2018;42.